Chapter 5

Fatty Acid and Phospholipid Crystalline Adsorbates: Steady State Studies *

To study the structural dynamics of molecular adsorbates on the surfaces, we used the Langmuir-Blodgett (LB) films. The LB technique was first introduced by Irving Langmuir and Katharine B. Blodgett in the 1930s [72, 73, 74]. Since then, it has proven powerful in the preparation of two-dimensional crystalline films [75, 76]. It allows for a controlled layer-by-layer deposition of ordered molecular films, and many different kinds of molecules have been successfully made into LB films. Because of the resemblance to naturally occurring biological membranes, lipid Langmuir films at water surfaces and Langmuir-Blodgett (LB) films often serve as a model system for studying membrane structures and properties under controlled conditions, such as head group organization and hydration [77], phase transitions [78], interactions with membrane proteins [79, 80], and proton diffusion [81]. And they are important in many other applications of technology developments, such as molecular electronics [82], biological sensors [83] and nonlinear optics [84]. The higher order and definite crystalline structure of LB films, compared with self-assembly, make them ideal for UEC studies.

However, the selective preparation of adsorbates with well-defined structures by means of the LB technique is not a trivial task [85, 86]. There was and still is

*This chapter is based on the work presented in references [28, 29, 71].

considerable effort in understanding the structure of even the "simplest" of all LB films, fatty acids and fatty acid salts (see reference [87, 88] for reviews). A plethora of powerful techniques (e.g., electron diffraction, neutron scattering, X-ray techniques, atomic force microscopy, FTIR, Raman spectroscopy, NMR) have been utilized to study the effect of the substrate [89, 90, 91], dipping conditions (for example, pH-value [86, 92, 93], pressure [94, 95, 96, 92, 97, 98], counterion [89, 90]) and the effect of the surfactant itself on the resulting film structure. Of particular interest are the tilting of fatty acids [94, 95, 97], structural differences in mono- and multilayers [99, 100, 101], epitaxial growth of fatty acids [102, 103, 104], and thermal annealing effects [103, 104, 105].

Phospholipids are the main building blocks of biomembranes and their molecular structures are similar to those of fatty acids. Although more complex and less studied, the structure of phospholipids LB films have been probed by a variety of techniques, including electron diffraction [106, 107, 108], X-ray diffraction [109, 77], infrared spectroscopy [110, 111], scanning tunneling microscopy (STM) [110, 112] and atomic force microscopy (AFM) [113].

5.1 Langmuir-Blodgett films of fatty acids and phospholipids

In general, fatty acid molecules (see for example the arachidic acid molecule shown in figure 5.1(A)) in LB films arrange in the following fashion: the long aliphatic chains pack with their axes parallel to each other but not necessarily perpendicular to the substrate surface (see figure 5.1(B)), as discussed in several articles [114, 96], reviews [87, 88] and monographs [75, 76, 115]. The C_2H_4 units form a sub-lattice with three possible different symmetries: orthorhombic (R), monoclinic (M) or triclinic (T). There are a number of possible variations of the sub-cell structure depending on the relative displacement of adjacent molecules, labeled by Miller indices of the interface layers. Moreover, depending on the nature of the substrate (for example, hydrophobic

or hydrophilic), and methods of interfacial preparation (for example, pH-value) the structure can vary.

The molecular structure of phospholipids (see for example dimyristoyl phosphatidic acid, i.e., DMPA, shown in figure 5.1(A)) is similar to that of fatty acids, but with some differences: two aliphatic chains instead of one, and a different headgroup. It is found that phospholipids organize in a two-dimensional hexagonal lattice where the aliphatic chains pack parallel to each other and perpendicular to the surface [106, 107, 108, 110, 111], as shown in figure 5.1(B). The structure of the C_2H_4 subunit cell is similar to that of the fatty acids.

Our observed diffraction patterns for these LB films of fatty acids and phospholipids are directly the result of the C_2H_4 subunit cell because of the covered s-range, s being the magnitude of the momentum transfer vector between the incident electron and the scattered electron. Different arrangements of the subunit cell can be uniquely distinguished by the measured lattice parameters and systematic absentees of certain Bragg spots. In this way we are able to establish the subunit cell structure, the in-plane orientation of the subunit cell with respect to the silicon surface and the out-of-plane direction of the aliphatic chains (i.e., inclination). Figure 5.2 depicts a schematic view of an orthorhombic C_2H_4 subunit cell — the depicted structure is from our diffraction analyses given below.

The thermal behavior of such films is of particular interest, especially when considering their two-dimensional structure on the substrate. Early studies of fatty acids have shown the onset of melting far below the bulk melting temperature and in multiple steps [116, 117, 118, 119, 120, 121, 122]. AFM has elucidated the two-dimensional melting and the structures involved [123, 124]. Multiple step melting was also observed in X-ray diffraction studies [125]. The transition from two-dimensional to three-dimensional melting in these fatty acid films, upon increasing the number of deposited layers, has been examined in a number of studies [126, 127, 128].

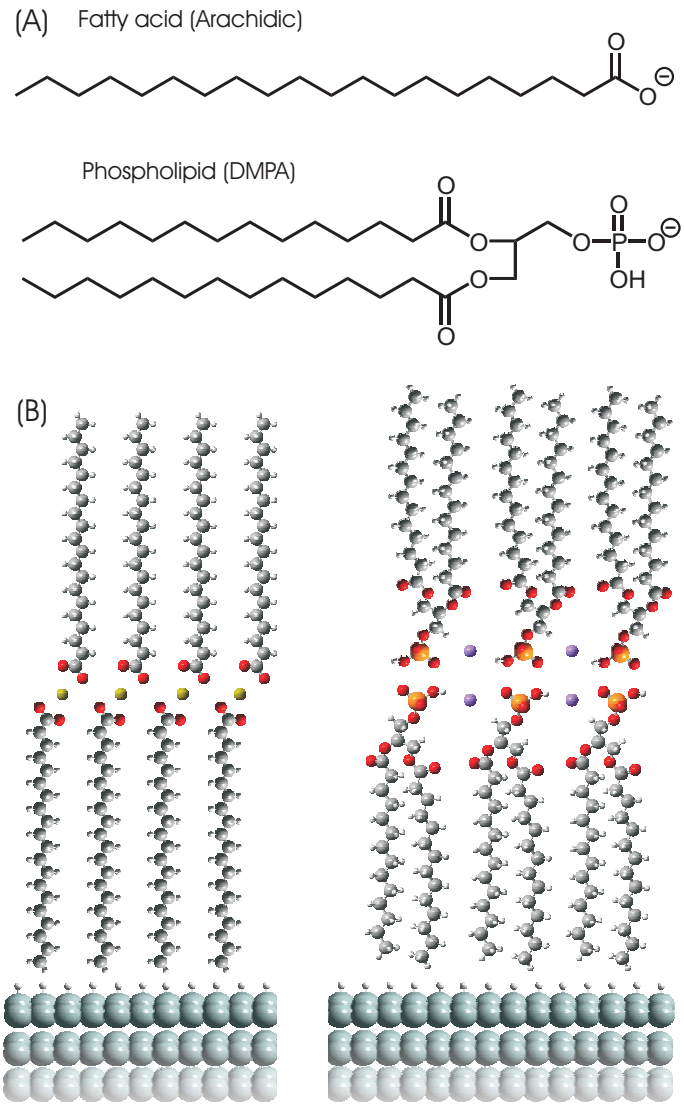

Figure 5.1: Structure of crystalline adsorbates of fatty acids and phospholipids.(A) The molecular structure of arachidic acid and DMPA. (B) Schematic side view of the two adsorbates on a hydrogen-terminated silicon(111) substrate. For the phospholipid and fatty acid, we show the bridging through the ions (salt); for the fatty acid, depending on pH, both the neutral and salt forms are present in the film [28, 29, 71].

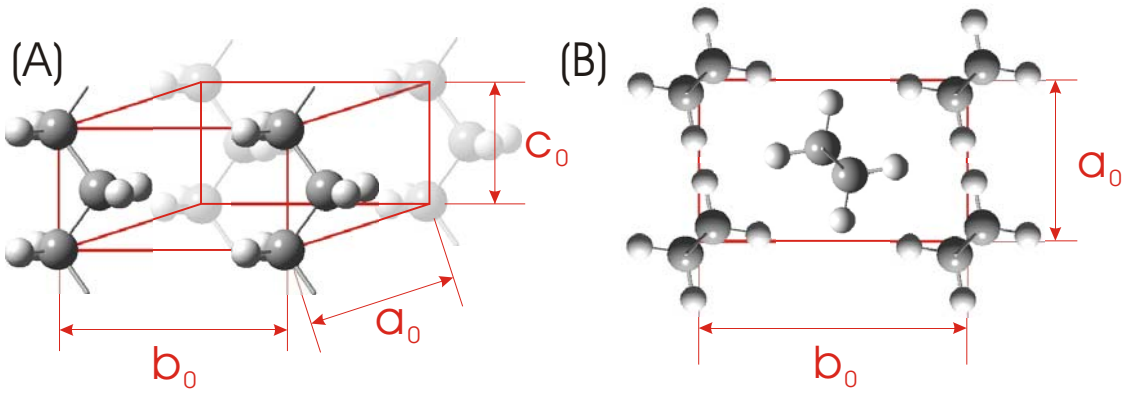

Figure 5.2: Structure of the orthorhombic C_2H_4 subunit cell. (A) The orthorhombic C_2H_4 subunit cell of aliphatic chains with lattice parameters a_0, b_0 and c_0. The chain at the center was omitted for clarity. (B) Top view of the orthorhombic subunit cell with lattice parameters a_0 and b_0 [28, 29, 71].

5.2 Preparation of layers by LB deposition

The substrate for all investigated samples was silicon(111). The surface was treated just before deposition, to be either hydrophilic or hydrophobic according to standard methods. Hydrophilic silicon surfaces were prepared by cleaning and oxidation with an RCA-1 solution. For the hydrophobic surfaces, subsequent etching of the oxide surface was made in a 40% NH_4F solution for 15–20 minutes in order to obtain the Si(111):H surface.

The deposition of the fatty acids and the phospholipids are in the so-called Y-geometry, i.e., head-to-head and tail-to-tail. For a hydrophilic surface, the first layer is attached to the surface by its hydrophilic head group; whereas for a hydrophobic surface, the first layer is attached by its hydrophobic tail. Since the film is always terminated by a hydrophobic tail, only odd numbered multilayers can be obtained for a hydrophilic substrate and even numbered multilayers for a hydrophobic substrate. We found that in order to achieve good film quality it was mandatory to prepare the LB films immediately after hydrogen-termination, because the hydrophobic silicon surface is unstable in air.

Arachidic acid (eicosanoic acid, $C_{19}H_{39}COOH$) was purchased from Aldrich and used without further purification (see figure 5.1(A)). The fatty acids were spread

from a chloroform solution. Prior to compression to the final deposition pressure, we allowed 20 minutes for complete evaporation of the solvent. For all samples the deposition took place in a NIMA LB trough at a dipping speed of 1 mm/min. The used subphase was an aqueous $CaCl_2$ solution (c[$CaCl_2$] = 0.5 mmol/liter, Millipore Water), which was adjusted to the desired pH value with aqueous diluted NaOH.

To study the influence of film thickness and dipping conditions, we prepared multiple samples of LB films at different pH values and dipping pressure. Two deposition pressures, $\pi = 10$ mN/m and $\pi = 29$ mN/m, were chosen for bilayer deposition. Although they gave the same condensed phase for the Langmuir films, it is found that deposition of fatty acid films with more than two layers failed at $\pi = 10$ mN/m. Here, we present selected bilayer samples deposited at $\pi = 10$ and 29 mN/m, and pH = 6.4, $\sim$7 and 9; and selected samples of 4- and 8-layer films deposited at $\pi = 29$ mN/m, and pH = 6.4, $\sim$7 and 9. At the pH values of 6.4 and 7, about 60% to 80% of the arachidic acid is deposited as the corresponding calcium salt, while at pH = 9, 100% of the arachidic acid is deposited as the salt [129].

To ensure a high sample quality the isotherms for the precursor Langmuir film and the transfer ratios upon deposition were routinely recorded. Furthermore, the morphology of the Langmuir film at the air-water interface was monitored with a Brewster Angle Microscope. For our dipping conditions, the Langmuir films were very uniform and did not show any macroscopic holes or multilayer islands.

In general, we recorded diffraction patterns of the LB films along two directions, which are perpendicular to each other. These correspond to the $[11\bar{2}]$ and $[\bar{1}10]$ zone axes of the underlying silicon substrate (see figure 5.3(A)), as evidenced from the diffraction patterns at high θ_i's. We denote these two directions with the azimuthal angle $\phi = 0°$ for $[11\bar{2}]$ and $\phi = 90°$ for $[\bar{1}10]$, respectively. Note, however, that we also have the ability to record diffraction patterns around these ϕ values in a range of at least $\pm 30°$. The deposition of the LB films was along either of these fundamental axes and accordingly we can distinguish a parallel ($\parallel$) or a perpendicular ($\perp$) dipping direction (see figure 5.3(B)). However, it is the silicon surface, rather than the dipping direction, which determines the structure and orientation of the fatty acid subunit

cell on the substrate, as discussed below.

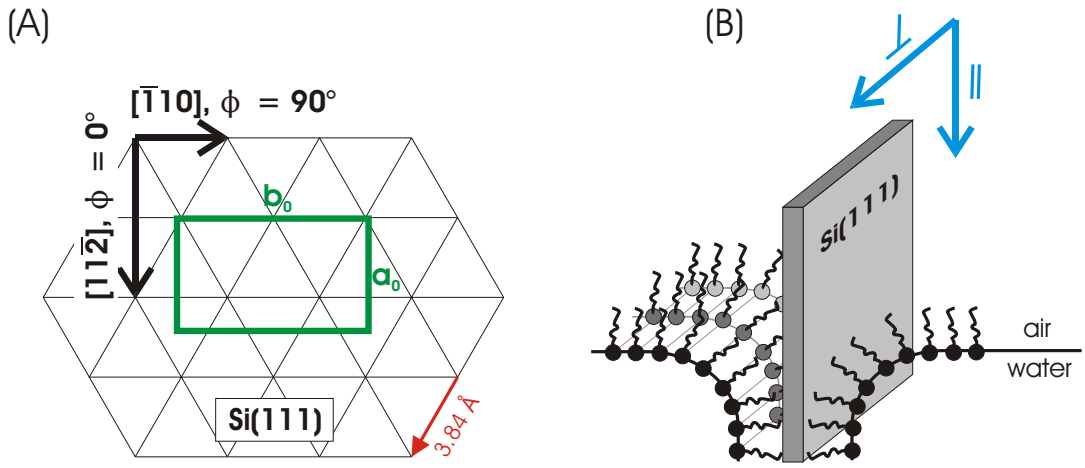

Figure 5.3: Directions of dipping, observation and subunit cell orientation. (A) Si(111):H surface lattice and the fatty acid C_2H_4 subunit cell, as observed in the diffraction experiments. (B) Deposition of a LB film results in two distinguishable directions: parallel ($\parallel$) and perpendicular ($\perp$) to the dipping direction [71].

For the phospholipids, 1,2-Dimyristoyl-*sn*-glycero-3-phosphate monosodium salt (dimyristoyl phosphatidic acid, DMPA) was purchased from Aldrich and used without further purification (see figure 5.1(A)). The lipids were spread from a chloroform/ methanol (3:1) solution, and the subphase used was Millipore water containing sodium ions at pH = 5.5. The deposition took place in a NIMA LB trough at a dipping pressure of $\pi = 29$ mN/m and a dipping speed of 1 mm/min. Film quality measurements were routinely recorded, as described above.

We prepared monolayers of dimyristoyl phosphatidic acid (DMPA) on a hydrophilic surface; the polar head groups are involved in bonding to the substrate. For the bilayers of DMPA, a hydrophobic substrate was utilized, in a similar fashion to the fatty acid samples. We used a hydrophilic oxide-terminated silicon(111) surface for the deposition of the monolayer and hydrophobic hydrogen-terminated silicon(111) surfaces for the bilayer. As in the case of the fatty acids, the deposition is in the Y-geometry.

Immediately after deposition the samples were transferred to ultrahigh vacuum

(UHV, $\sim 10^{-10}$ torr), where all the experiments were carried out. The LB films are stable under electron exposure, as evidenced by the absence of change or deterioration in the quality of the static diffraction patterns. However, prolonged laser irradiation and increased static sample temperature can lead to change or even loss of the diffraction patterns, as described below.

5.3 Fatty acid bilayers structure

The static diffraction patterns of bilayer films are shown in figure 5.4(A), (B) and (C). The panels are for LB films prepared at different conditions but all observed by UEC, i.e., recorded with ultrashort electron pulses, but without the laser heating pulse. The top panels show the diffraction patterns observed at $\phi = 0°$, while the bottom ones show diffraction patterns observed at $\phi = 90°$, all at low incidence angles $\theta_i < 1°$. Panel (A) displays the diffraction patterns for the bilayer deposited at pH = 9 and $\pi = 10$ mN/m when dipping occurred along the $[11\bar{2}]$ direction of silicon. Panel (B) displays diffraction patterns for the bilayer deposited at pH = 6.4 and $\pi = 29$ mN/m when dipping occurred along the $[\bar{1}10]$ direction of silicon. Panel(C) displays diffraction patterns for the bilayer deposited at pH $\simeq$ 7 and $\pi = 29$ mN/m when dipping occurred along the $[\bar{1}10]$ direction of silicon.

The diffraction patterns are all composed of well resolved Bragg spots. This is the result of a high quality crystalline structure of the bilayers. The rectangular arrays of spots are perpendicular to the shadow edge. It follows that the aliphatic chains pack with their chain axes parallel to each other and perpendicular to the substrate surface.

In figure 5.4, the bright spots above the shadow edge (not indexed) are due to the main reflection beam Si(00) from the substrate silicon. This was confirmed from the θ_i dependence (rocking curve) which shows large changes for these bright spots but not for the bilayer adsorbate. Figure 5.5 depicts this behavior for the substrate and for the bilayer deposited at $\pi = 10$ mN/m and pH = 9, and whose static diffraction patterns at small θ_i's are shown in figure 5.4(A). It is clear that while the LB(002)

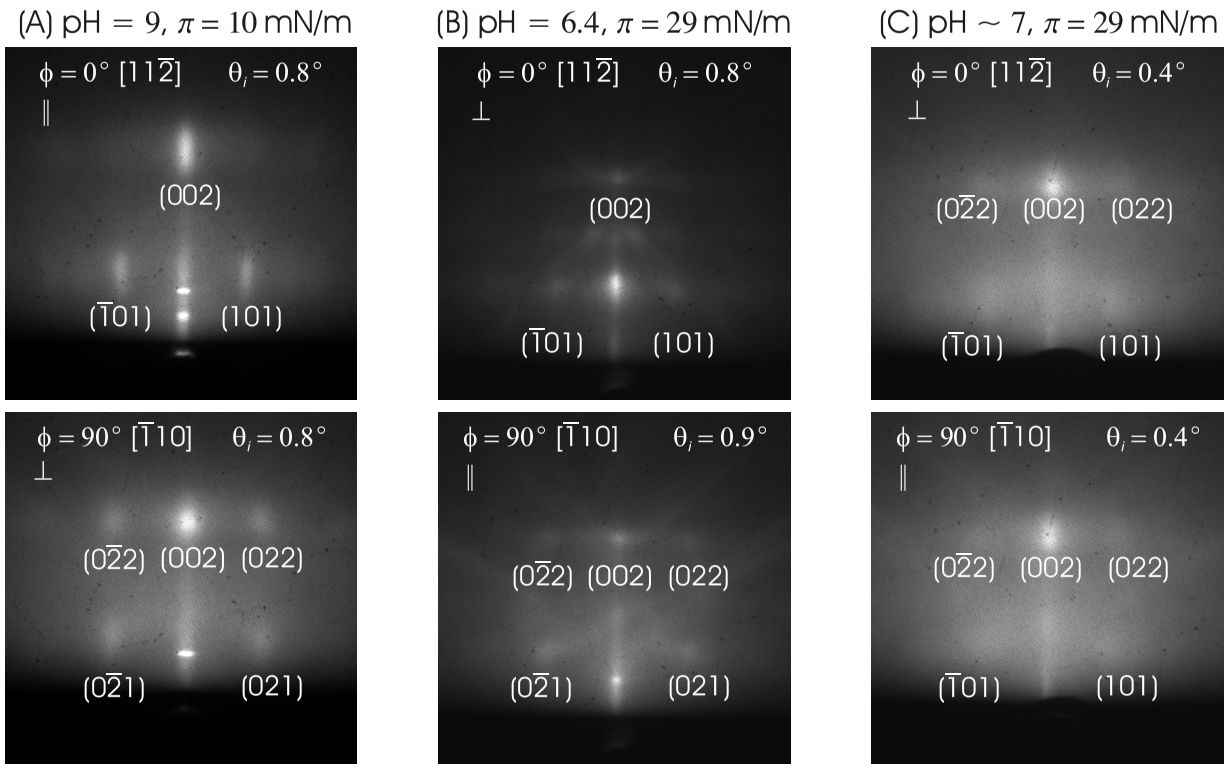

Figure 5.4: Static diffraction patterns of fatty acid bilayers at $T = 295$ K. The s range for all diffraction patterns is from -0.6 to +0.6 Å^{-1} in the horizontal direction and from 0 to +1.2 Å^{-1} in the vertical direction.(A) Diffraction patterns for the bilayer deposited at pH = 9 and $\pi = 10$ mN/m, where the incidence angle is $\theta_i = 0.8°$ for $\phi = 0°$ and $\phi = 90°$. (B) Diffraction patterns for the bilayer deposited at pH = 6.4 and $\pi = 29$ mN/m where the incidence angle is $\theta_i = 0.8°$ for $\phi = 0°$ and $\theta_i = 0.9°$ for $\phi = 90°$. (C) Diffraction patterns for the bilayer deposited at pH $\simeq$ 7 and $\pi = 29$ mN/m where the incidence angle is $\theta_i = 0.4°$ for $\phi = 0°$ and $\phi = 90°$[71].

spot remains at the same s position (near $s = 0.8$ Å^{-1} in figure 5.5), the Si(00) peak position changes periodically with θ_i, showing the higher orders of the Si(111) Bragg diffraction.

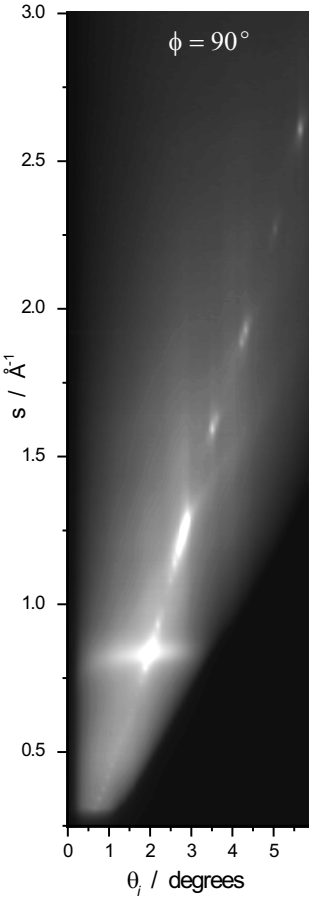

Figure 5.5: Experimental rocking curve for the z-component of the scattering vector s (from +0.25 to +3.0 Å^{-1}) vs. incidence angle θ_i (0 to 5.85°) at $\phi = 90°$, showing the (002) peak (see diffraction near $s = 0.8$ Å^{-1}) of the bilayer and (00) peak of the Si(111) surface (at higher s-values) [28, 71].

The rocking curves — θ_i changes — give insight into the overall order of the bilayer, and similarly the ϕ changes. The patterns do not change considerably when rotated in a range of ±14° about both $\phi = 0°$ and $\phi = 90°$ direction. The Bragg spots remain at their positions as shown in figure 5.4; only the intensities undergo a small change. Further increase of the angle ϕ results in extension of the Bragg spots into lines parallel to the shadow edge. These behaviors, as well as the rectangular arrays of the spots suggest that the diffraction patterns are formed by electrons transmitted

through the bilayer (see section 3.1). It also infers that the fatty acid bilayers are textured samples. There are small domains of the crystalline fatty acid molecules. While they have the same out-of-plane direction with all the chains perpendicular to the substrate surface, they have slightly different in-plane orientations.

The rocking curve indicates two important points to be made regarding differences in two-dimensional and three-dimensional crystal behavior. First, at large θ_i values, the electrons penetrate the bulk and we observe the higher orders of Bragg diffraction of the substrate. In fact it is from these high-order diffractions that we can determine the lattice spacing of the used substrate. At lower values of θ_i, the spots are stretched diagonally, making the substarte spacing less accurate to determine. At the lowest θ_i, the pattern is dominated by the adsorbate diffraction features. The behavior with θ_i of an adsorbate spot shows insensitivity in the region of θ_i studied.

This brings to focus the second point regarding measurements of rocking curves. Unlike three-dimensional crystals, two-dimensional systems exhibit "rods" in the diffraction reciprocal space. As the layers build up in thickness, the rods are modulated by the inverse chain distance of c_0. Thus, for two-dimensional systems the intensity should not change drastically with θ_i, while for three-dimensional systems they will. From the horizontal width of our diffraction ($\Delta s \simeq 0.06$ Å^{-1}), we obtain a nm scale coherence length. Moreover, the vertical width of Δs gives a maximum inhomogenity in -CH_2-CH_2-CH_2- distances of $\sim$20%, relative to the 2.54 Å distance of c_0.

From the positions of the Bragg spots (including systematic absentees), the subunit cells were determined to be orthorhombic, with short notation of R(001). Accordingly, "R" represents the orthorhombic symmetry and (001) is for denoting the (ab) plane of the C_2H_4 subunit cell which is parallel to the substrate Si(111) surface. Basically, the vertical s spacing gives the c_0 values while side diffractions give a_0 and b_0 for the two ϕ's, respectively. Note that the direct beam is located below the shadow edge.

Figure 5.6 shows the simulated diffraction patterns of an orthorhombic, infinite crystal of aliphatic carbon chains for the [100] and [010] direction, which are the two directions studied in the experiments. Indeed the patterns show the characteristic

spots as in figure 5.4, with the same symmetry, spacings and absentees. Although the intensities of the calculated Bragg spots, especially for $(\bar{2}02)$ and (202), do not reproduce those measured. This is because the calculation was made for an infinite array of chains in the crystal and the underlying substrate and the headgroups were not taken into account, and it was not scaled with the s-decay of diffraction.

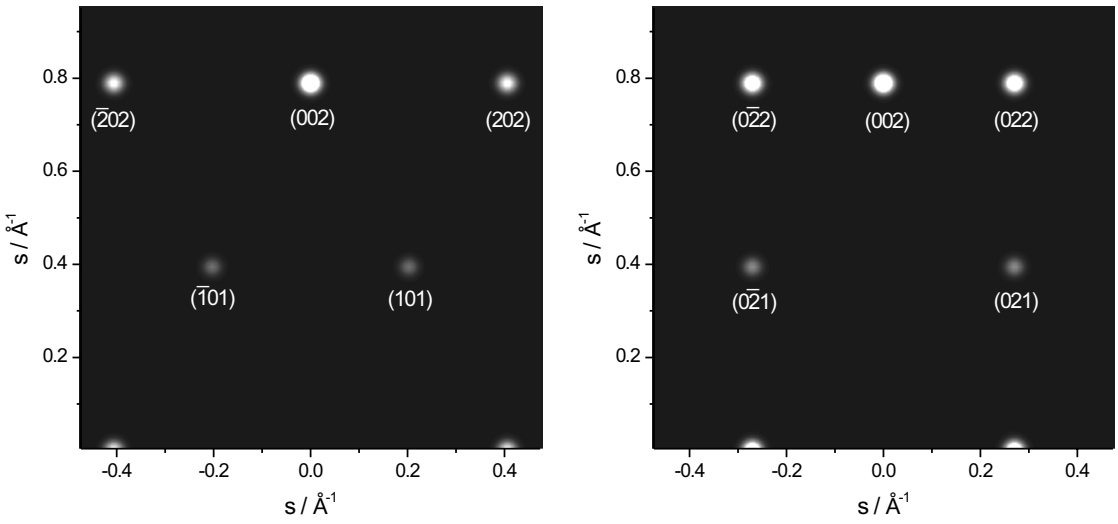

Figure 5.6: Calculated diffraction patterns of an orthorhombic, infinite crystal of aliphatic carbon chains observed along the [100] and [010] direction, respectively. The subunit cell lattice parameters used are $a_0 = 4.93$ Å, $b_0 = 7.4$ Å and $c_0 = 2.534$ Å. The space group is V_h^{16} (Pnam) [71].

The determined lattice parameters of the different bilayer structures are summarized in Table 5.1. The lattice parameters c_0, which result from the vertical s-spacing of the Bragg spots, have the same magnitude for all three samples. They agree well with the theoretical value of 2.54 Å, which follows from a simple geometrical consideration for an aliphatic chain with bond distances $r_{\text{c-c}} = 1.53$ Å and angle $\angle_{\text{c-c-c}} = 112°$. The c_0 value represents the distance between CH_2 planes, and it holds true for the 4- and 8-layer samples, as shown below.

The determined a_0 and b_0 values vary for different conditions and range for a_0 from 4.7 to 4.9 Å; and for b_0 from 8.0 to 8.5 Å. These values differ somewhat from the theoretical values of $a_0 = 4.96$ Å and $b_0 = 7.4$ Å [115], which were estimated, by

	pH = 9, π = 10 mN/m (figure 5.4(A))	**pH = 6.4, π = 29 mN/m (figure 5.4(B))**	**pH $\simeq$ 7, π = 29 mN/m (figure 5.4(C))**
a_0/ Å	4.7	4.9	4.7
b_0/ Å	8.0	8.3	8.5
c_0/ Å	2.54	2.59	2.57

Table 5.1: Lattice parameters determined for the fatty acid bilayer samples prepared differently.

purely geometrical considerations, for the ideal case of closest packed arrays of infinite aliphatic chains. The difference can be explained by the fact that the theoretical values do not take into account the carboxylic end groups of fatty acids. Moreover the substrate and the deposition conditions all have an important role in the order at the interface.

While the parameter a_0 has a similar value for all bilayer samples, b_0 is slightly larger for the samples prepared at lower pH values (pH = 6.4 and $\sim$7 vs. pH = 9) and higher pressures (π = 29 mN/m vs. π = 10 mN/m). Though the pressure has little effect on the molecular packing in this range, as observed in the π-area isotherm, it has been observed that the pH value has a rather strong influence on the overall packing of the LB film. An increase of the pH value is believed to pull the head-groups closer together and support a nontilted LB film structure [92]. In the sample deposited at pH = 9, virtually all fatty acid molecules are in their salt form, which leads to a slightly closer packing compared to the deposited structures at lower pH values, where only 60%–80% of the fatty acids are in their salt form [129].

By comparing figure 5.4(A) and (B) we notice that the orthorhombic subunit cell is always aligned with its b_0-axis along the $[\bar{1}10]$ direction of the Si(111) surface and, thus, the a_0-axis is along the $[11\bar{2}]$ direction, regardless of the dipping direction. This influence of the substrate is expected and has been noted for hydrogen-terminated Si(111) [130]. In this context, it is worth noting that the structure of the precursor Langmuir film, i.e., the monolayer on water, has relatively less influence on the structure of deposited LB films [102, 88, 131].

The influence of the substrate explains the orientational ordering of the adsorbate

on the substrate, as is illustrated in figure 5.3(A). The length of one repetitive unit along the $[\bar{1}10]$ and $[11\bar{2}]$ direction of silicon substrate, which are 3.84 and 6.65 Å in real space, respectively, are to be compared with b_0 and a_0 of the adsorbate layer. Two repetitive units along the $[\bar{1}10]$ direction correspond to 7.68 Å, a value which is close to the observed $b_0 = 8.0$ Å (and 8.3 Å). The length mismatch is only 4% (and 8%). If b_0 was oriented along the $[11\bar{2}]$ direction, then, because the distance of repetitive units is 6.65 Å, the mismatch would be 20% to 25%. The disagreement between a_0 of the orthorhombic subunit cell and the lattice parameters of silicon is $> 20\%$ in either orientation. It is therefore reasonable to explain, because of this length correlation, the b_0 axis alignment along the $[\bar{1}10]$ direction of the substrate, and thus the orientation is independent of the dipping direction and the precursor Langmuir film structure.

This orientation is also sensitive to substrate structure. In figure 5.4(C), the observed diffraction patterns form no "perfect" rectangular array of Bragg spots and the diffraction patterns in the two distinct directions of $\phi = 0°$ and $\phi = 90°$ are similar and differ only in intensity and sharpness of the spots. This is in stark contrast to the distinct diffraction patterns in the two directions for the samples shown in figure 5.4(A) and (B) and the predicted patterns in figure 5.6. Close inspection of the diffraction patterns in figure 5.4(C) reveals that they result from a superposition of the two diffraction patterns ($\phi = 0°$ and 90°) displayed in figure 5.6. This loss of preferred orientation is consistent with the fact that the diffraction patterns do not change their general form upon rotation in a range of at least $\phi = \pm 30°$ in both directions. In this particular sample the absence of the alignment is believed to originate from a partial oxidization of the surface prior to dipping; hydrogen-terminated silicon surfaces are known to be easily oxidized in air.

In summary, calcium arachidate bilayers form orthorhombic structure on the hydrophobic Si(111) substrate, with the fatty acid chains aligned perpendicular to the surface. The C_2H_4 subunit cell is determined to be R(001) and all the lattice parameters are extracted. Samples prepared at higher pH values showed a closer packing of the fatty acid. The substrate surface has a large influence on orientation, and in

this case the b_0-axis is along the $[\bar{1}10]$ direction of the hydrogen-terminated Si(111) surface and the a_0-axis along the $[11\bar{2}]$ direction.

5.4 Fatty acid bilayers temperature-dependent structural change

Following characterization of structures we studied the effect of substrate temperature. For the bilayer sample deposited at $\pi = 29$ mN/m and pH $\simeq$7, diffraction patterns at $\phi = 0°$ were recorded at different temperatures in the range from $T = 100$ to 380 K; representative examples of diffraction patterns are shown in figure 5.7 for $T = 100, 295, 333$ and 370 K. The patterns are indexed as described above and displayed on the $T = 100$ K pattern. The diffraction pattern shows Bragg spots as in figure 5.4 and is very clear at 100 K. The patterns become more diffuse with increasing temperature; the intensity of Bragg spots decreases while the background gains intensity. At 370 K, just below the melting temperature of arachidic acid salt LB films of $\sim$383 K [120], the characteristic features of spots are barely visible in the patterns. This shows that the temperature increase is responsible for the enhanced thermal and inhomogeneous disorder, leading ultimately to a total randomness and breakdown of the bilayer structure at the melting point.

The relative (integrated) intensity change I/I_0 of the (002) Bragg spot as a function of temperature is shown in figure 5.8(A). An intensity drop is expected by the Debye-Waller effect due to increased thermal motions of the scattering atoms with increasing temperature. These motions have direct influence on structural factors. However, it is remarkable that the intensity drop shown in figure 5.8(A) features certain temperature points at which the slope abruptly changes (shown in the inset). Such a thermal behavior is different from conventional melting of isotropic bulk materials and could be related to phase transitions, as observed with AFM [123, 124], of two-dimensional, anisotropic LB films.

In diffraction, besides the Debye-Waller intensity drop, one expects a sharp de-

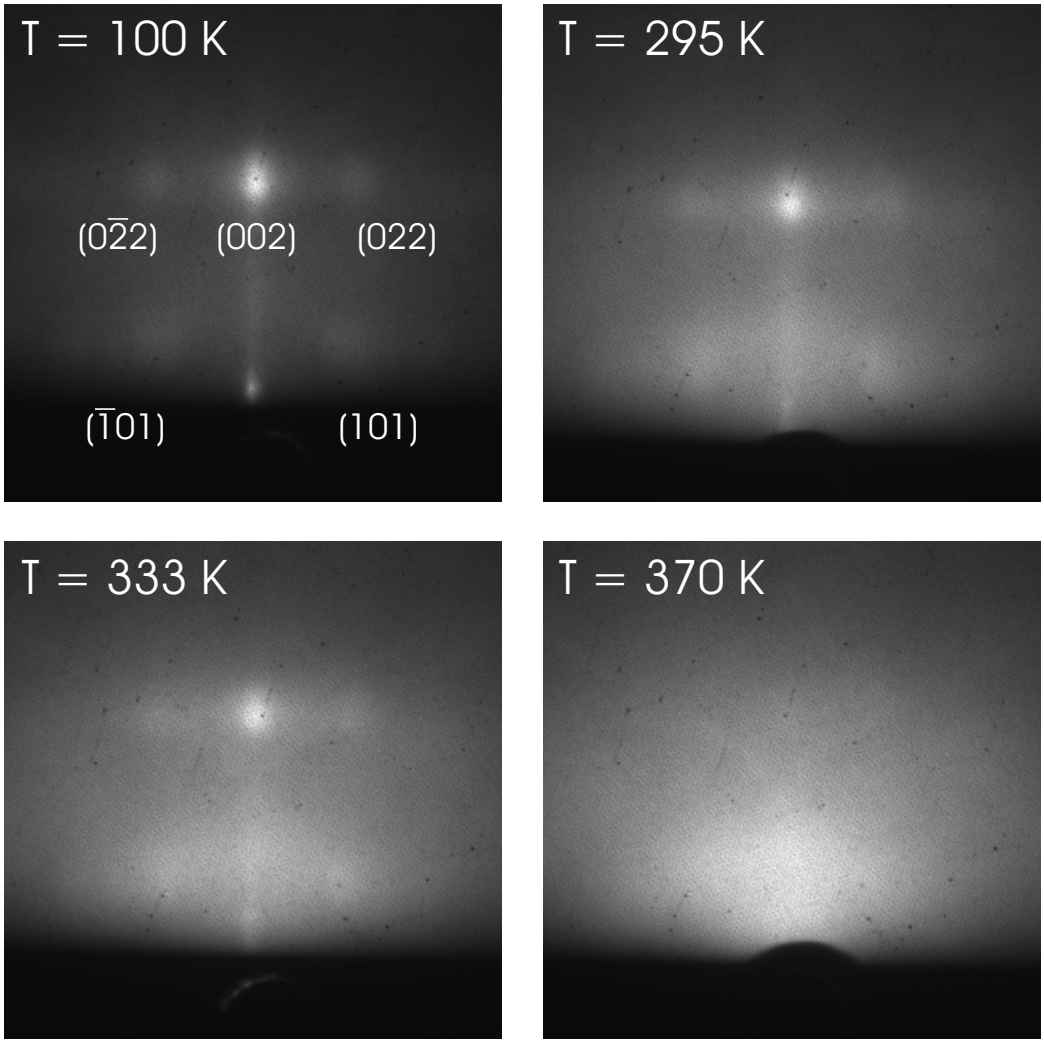

Figure 5.7: Static temperature dependent diffraction patterns for the calcium arachidate bilayer deposited at pH $\simeq$ 7 and $\pi = 29$ mN/m at $T = 100, 295, 333$ and 370 K. The patterns are observed at $\phi = 0°$ and $\theta_i = 0.4°$. The s range for all diffraction patterns is from -0.6 to +0.6 Å^{-1} in the horizontal direction and from 0 to +1.2 Å^{-1} in the vertical direction [71].

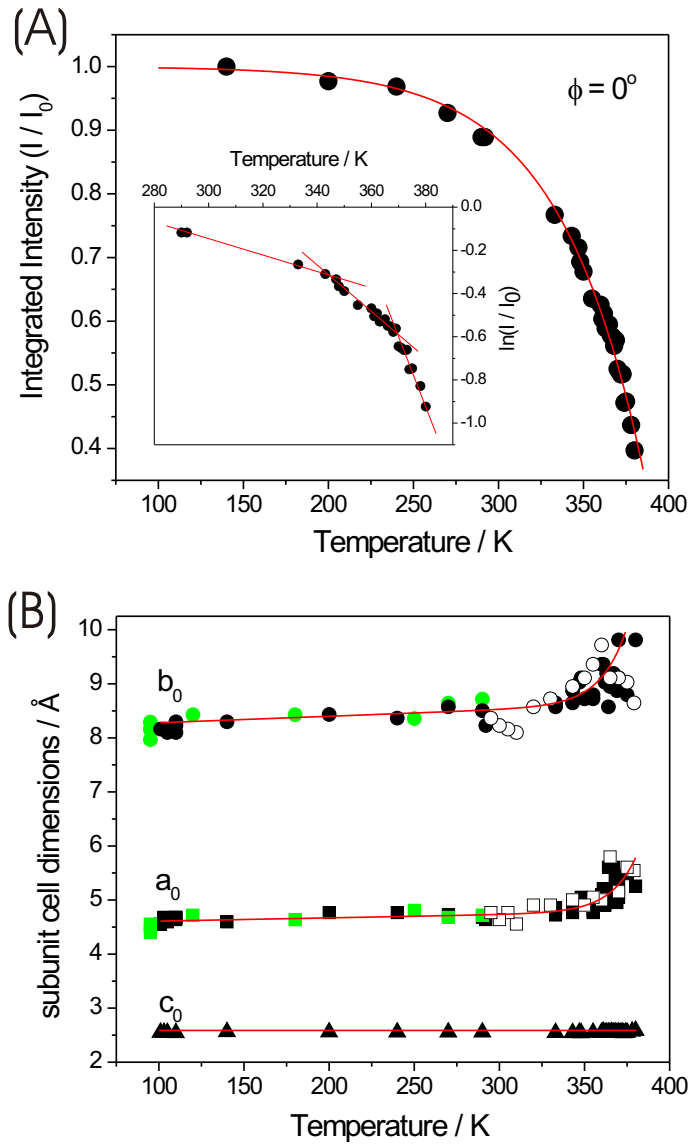

Figure 5.8: Static temperature dependence of diffraction intensity and subunit cell dimensions (Å) for the calcium arachidate bilayer deposited at pH $\simeq$ 7 and π = 29 mN/m. (A) Relative intensity change I/I_0 of the (002) spot in the temperature range from T = 140 to 380 K observed at $\phi = 0°$ and $\theta_i = 0.4°$. The inset emphasizes the abrupt slope changes in a plot of $ln(I/I_0)$ against temperature in the range from 280 to 380 K. (B) Change of the subunit cell parameters a_0, b_0 and c_0 observed at $\theta_i = 0.4°$. The black symbols represent cell parameters observed at $\phi = 0°$, whereas the open symbols denote cell parameters observed at $\phi = 0°$ after cooling down from T = 380 K. The green symbols stand for the subunit cell parameters obtained at ϕ = 90° from T = 95 to 290 K. The red line is a guide for the eye [71].

crease in intensity if a phase transition is present, such as in conventional melting. However, this transition is only sharp if the layers are thick enough to define a three-dimensional collective behavior. For two-dimensional melting, pretransitional disordering in the form of thermally-induced random tilt and/or bending of the aliphatic chains [120] erodes the sharpness and renders the transition to occur over a wider temperature range. This picture of disorder involves several steps, first disordering of the hydrocarbon tails and then the breakdown of the head-group region, the latter occurs at the main melting point [116, 117]. Raman studies also support the presence of pretransitional regions [132].

The effect of static temperature on the subunit cell parameters is shown in figure 5.8(B). With increasing temperature, the film expands along a_0 and b_0, first slowly then more rapidly with an onset of $\sim$50 K below the bulk melting point. A similar behavior has been reported for a fatty acid salt LB film [121], however, the expansion reported here is significantly more pronounced. It should be noted that the guide for the eye (red line) has the same shape for a_0 and b_0 but is only shifted along the y-axis of the figure, indicating a similar expansion in a_0 and b_0 of $\sim$25% in the range from 100 to 380 K.

The expansion of the subunit cell in the plane parallel to the substrate surface is fully reversible as long as the sample is heated to temperatures below or near the bulk melting point and for a short time (minutes). In figure 5.8(B) the open circles and squares indicate that the initial cell parameters are retrieved after cooling down. However, the intensity of the Bragg spots recovers only partially (not shown), indicating some loss of crystalline order in the LB film. Within our accuracy no expansion is observed along c_0, i.e., along the fatty acid chains.

In summary, with increasing temperature we observed a pronounced loss of Bragg spot intensity, but with behavior much different from what is expected from the Debye-Waller effect for a bulk material. Rather, the behavior reflects the two-dimensional pretransitional structural changes. We also observed an in-plane expansion of the subunit cell of the chains, together with increased lateral (in-plane) disorder, as evidenced in the buildup of background scattering. At the same time

the degree of order in the carbon chains decreases. These processes are partially reversible as long as the temperature is below the main melting point. Beyond the main melting point the head-group region breaks down and the crystalline order of the adsorbate is lost. A structural picture is depicted in figure 5.9.

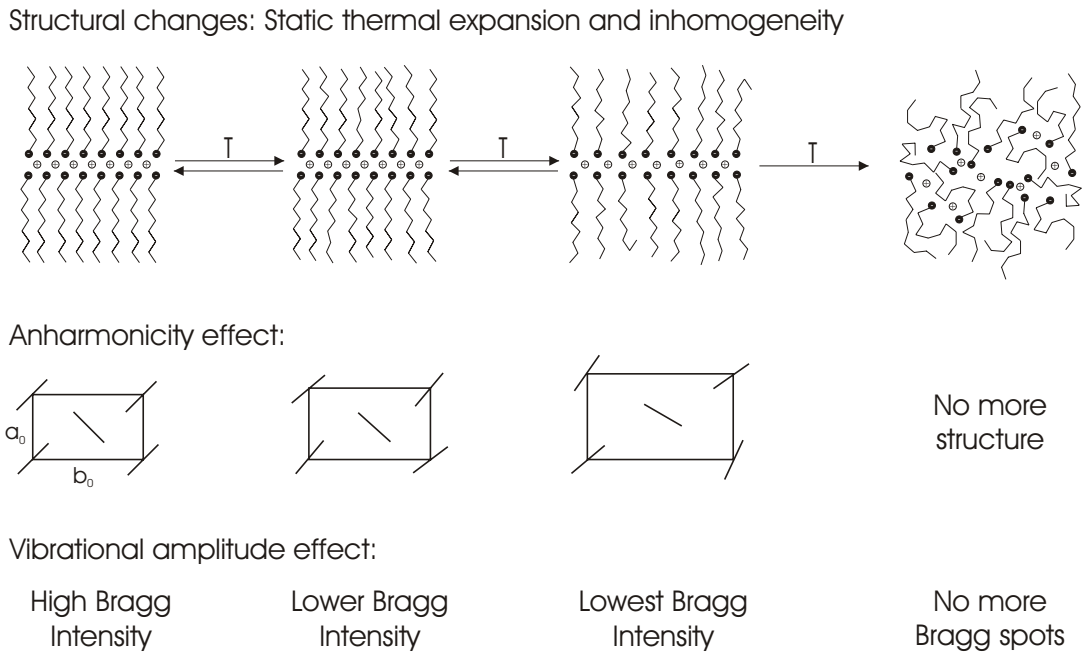

Figure 5.9: Schematic view of the static thermal behavior for changes of a bilayer with temperature increase [71].

5.5 Fatty acid multilayers structure

The static diffraction patterns recorded at room temperature for 2-, 4- and 8-layer samples deposited at pH = 6.4 and π = 29 mN/m are shown in figure 5.10. The upper panels show the diffraction patterns observed along the silicon $[11\bar{2}]$ direction ($\phi = 0°$, $\perp$), and the lower panels show the patterns along the silicon $[\bar{1}10]$ direction ($\phi = 90°$, $\|$). All diffraction patterns take the form of rectangular arrays of spots, and are indexed from the positions of the Bragg spots, as shown for the bilayer (see figure 5.4(B) and also figure 5.6). The indexing is the same for the 4- and 8-layer samples, but omitted in the figure for clarity. The fatty acid molecules arrange in an

orthorhombic R(001) packing with the subunit cells b_0-axis aligned along the silicon $[\bar{1}10]$ direction for all samples independent of layer thickness.

The extracted subunit cell parameters are summarized in Table 5.2. Within the error bars, the 2- and 4- layer samples have the same lattice parameters, possibly because of the strong influence of the underlying substrate. With more deposited layers this influence becomes weaker and results in the slight expansion of b_0 in the 8-layer sample by ∼8% compared to the 2-layer sample; a_0 remains unaltered in the 8-layer sample. This can be explained as follows: because b_0 is the direction of better match (stronger interaction) with the substrate the change is larger in this direction as layers become further away from the surface. On the other hand, an increase of "defects" and holes, when multiple layers are deposited [88], can also lead to a relaxation of the observed film structure. The Bragg spots are not as sharp for the 8-layer sample as they are for the 2- and 4-layer ones, and this behavior is consistent with some loss of order of crystallinity to randomly oriented crystallites, as has been observed for behenic acid multilayers [103, 104]. However, the aliphatic chains are still aligned nearly perpendicular to the sample surface and keep their stacked arrangement.

	2-layer	**4-layer**	**8-layer**
$\mathbf{a}_0$/ **Å**	4.86	4.87	4.85
$\mathbf{b}_0$/ **Å**	8.28	8.33	8.91
$\mathbf{c}_0$/ **Å**	2.59	2.54	2.54

Table 5.2: Lattice parameters for the 2-, 4- and 8-layers deposited on the hydrophobic substrate of Si(111) surface: pH = 6.4 and π = 29 mN/m.

Before IR laser ($\lambda = 800nm$) irradiation, the 8-layer sample gives the diffraction pattern shown in figure 5.11(A) for $\phi = 0°$. Upon laser annealing this sample recovers the diffraction pattern shown in figure 5.11 and is that of figure 5.10. The pattern before annealing is basically characteristic of the film but along an "inclined line" (by ∼20°), reflecting partial inclination of the chains; the annealing leads to the disappearance of such a tilt and the structure becomes that of a perpendicular chain geometry. However, another 8-layer LB film prepared at pH $\simeq$ 7 and π = 29 mN/m,

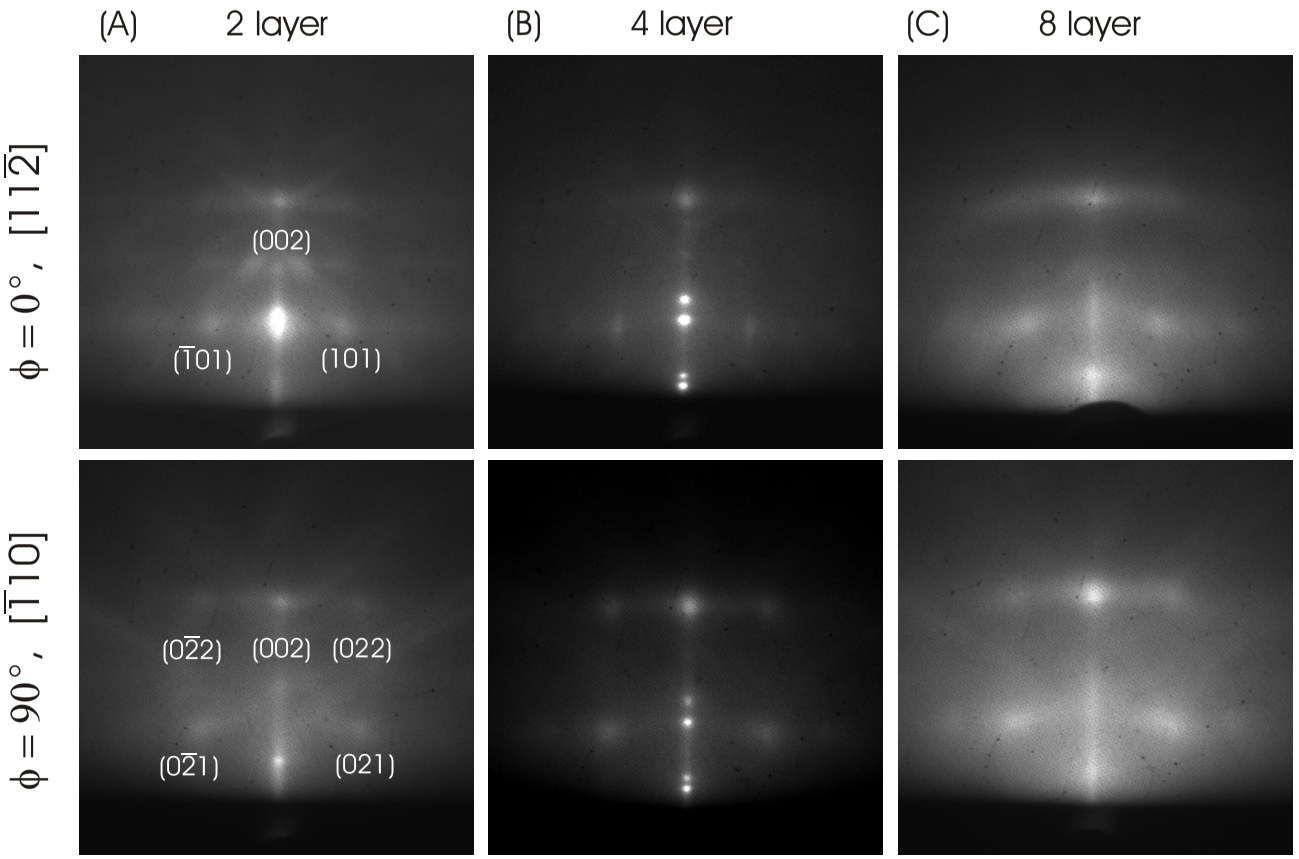

Figure 5.10: Diffraction patterns obtained for the calcium arachidate LB films of (A) 2-, (B) 4- and (C) 8-layers deposited at pH = 6.4 and π = 29 mN/m. Deposition occurred along the [$\bar{1}$10] direction of silicon. The incidence angles for the patterns observed at $\phi = 0°$ (upper panels) are θ_i = 0.8°, 0.8°, 0.5° for 2-, 4-, and 8-layers, respectively, and for $\phi = 90°$ (lower panels) they are θ_i = 0.9°, 0.4°, 0.4°. The s range for all diffraction patterns is from -0.6 to +0.6 Å^{-1} in the horizontal direction and from 0 to +1.2 Å^{-1} in the vertical direction [71].

although showed clearly the partial inclination, it did not change upon laser irradiation, as is apparent in the static diffraction pattern shown in figure 5.11(B), which shows the persistence of the inclined feature. Two parallel lines with a tilt angle of ∼10° to the right were observed at both $\phi = 0°$ and $\phi = 90°$.

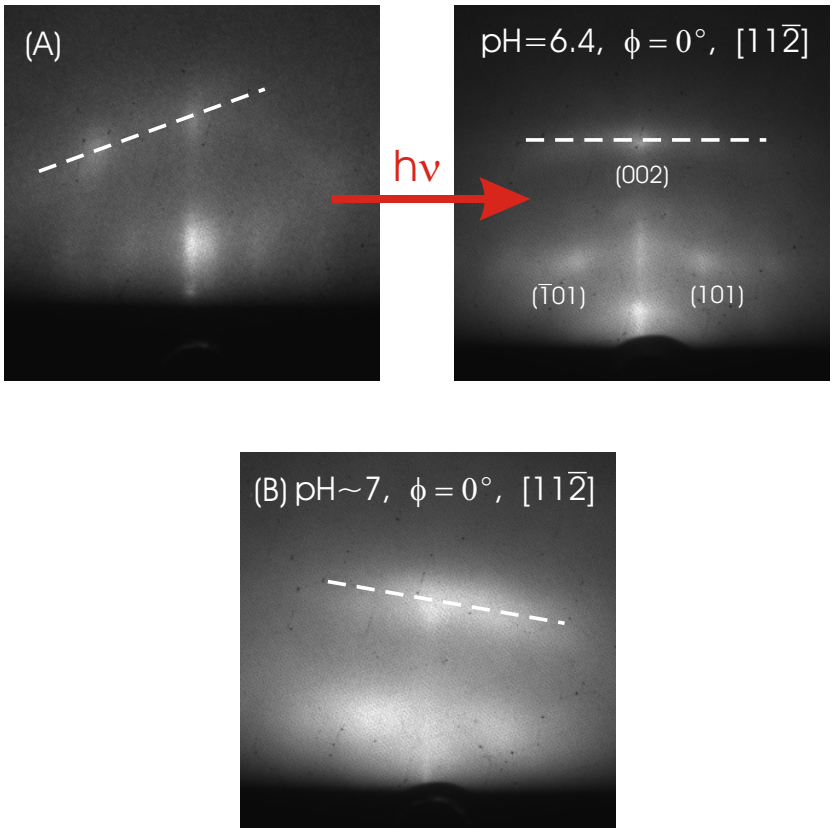

Figure 5.11: Inclined diffraction patterns for 8-layer samples at $\phi = 0°$, with the s-range from -0.6 to +0.6 Å^{-1} in the horizontal direction and from 0 to +1.2 Å^{-1} in the vertical direction. (A) The 8-layer sample deposited at pH = 6.4 and $\pi = 29$ mN/m shows a partial inclination of ∼20° to the left (dotted line), which vanishes after laser irradiation. The incidence angle is $\theta_i = 0.4°$. (B) The 8-layer sample deposited at pH $\simeq 7$ and $\pi = 29$ mN/m shows a partial inclination of ∼10° to the right, which for this sample is stable with laser irradiation. The incidence angle is $\theta_i = 0.5°$ [71].

The spacing between the inclined lines along the tilted direction gives again $c_0 = 2.54$ Å, consistent with results to all samples studied. Besides the smeared lines some Bragg spots are apparent, most notably the (002) reflection, however lateral order could not be extracted. This change into an inclined chain structure is consistent

with results showing that LB films composed of a few layers of fatty acid salts have an upright arrangement, whereas multilayers possess an inclined carbon chain geometry [88].

In summary, the static structures of 2-, 4-, and 8-layer samples of calcium arachidate are rather similar, though inclination of the fatty acids together with an increase in disorder begins to show in the 8-layer samples. The influences of substrate orientation and interaction decreases as more layers are formed in the structure.

5.6 Phospholipid monolayer and bilayer structure

In figure 5.12(B) and (C), the static diffraction patterns for DMPA monolayers and bilayers are depicted, respectively. The two patterns are very similar and their strongest feature is a horizontal diffraction (curved) line, which is labeled by the Miller indices ($hk2$). Since the line is basically the composite of Bragg diffractions in the second diffraction order (compared to the diffraction pattern of fatty acids shown in figure 5.12(A)), we are able to determine the subunit cell parameter c_0 to be 2.54 Å from the s value in the vertical direction. This again is expected because of the covalent -CH_2-CH_2-CH_2- distances involved in the aliphatic chains of DMPA, which are essentially the same as in arachidic acid (see figure 5.1(A)). The patterns indicate that the aliphatic chains are packed parallel to each other and are aligned nearly perpendicular to the surface.

However, long-range in-plane order was not observed, as we could not resolve separate Bragg spots, as we did for the fatty acids. This limited resolution may be due to the fact that the more complex chemical structure of DMPA does not allow the molecules to pack as easily into orthorhombic (or other symmetries) crystals over an extended area. The crystallinity of the film is more restricted; "bulk" crystals of DMPA show inclination $\beta = 114.2°$ of the carbon chains [133], whereas in the adsorbate DMPA on the substrate the chains are forced to be nearly perpendicular to the surface. Diffraction patterns also show diffuse scattering in the lower s range. The independence of the diffraction patterns on electron incidence angle θ_i and the

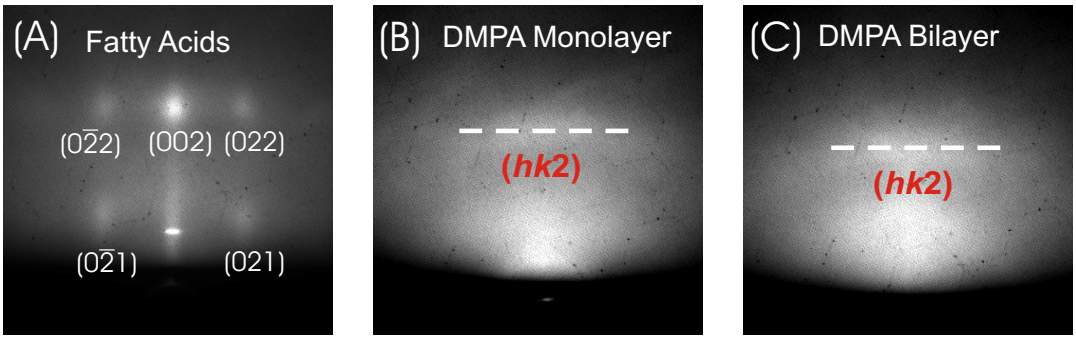

Figure 5.12: The diffraction patterns of fatty acids (A), DMPA monolayer (B) and bilayer (C) samples. The incidence angle is $\phi = 90°$ and $\theta_i = 0.8°$ for fatty acids (A), $\phi = 90°$ and $\theta_i = 0.7°$ for DMPA monolayer (B) and $\phi = 0°$ and $\theta_i = 0.5°$ for DMPA bilayer (C) [29, 71].

azimuthal angle ϕ is consistent with the existence of polycrystalline domains.